

*Electronic supplementary information*

**Strong Metal-Support Interactions between Palladium Nanoclusters and Hematite toward Enhanced Acetylene Dicarboxylation at Low Temperature**

Xuemei Wei<sup>a,b</sup>, Zhanwei Ma<sup>a</sup>, Jinzhi Lu<sup>a,b</sup>, Xinyuan Mu<sup>a</sup>, Bin Hu<sup>a\*</sup>

*<sup>a</sup>State Key Laboratory for Oxo Synthesis and Selective Oxidation, Lanzhou Institute of Chemical Physics, Chinese Academy of Sciences, Lanzhou 730000, China*

*<sup>b</sup>University of Chinese Academy of Sciences, Beijing 100049, China*

**Summary**

|                                                              |    |
|--------------------------------------------------------------|----|
| Materials and chemicals.....                                 | 2  |
| $\alpha$ -Fe <sub>2</sub> O <sub>3</sub> @C preparation..... | 2  |
| SchemeS1.....                                                | 2  |
| Catalyst characterization.....                               | 3  |
| Fig. S1.....                                                 | 4  |
| Table S1.....                                                | 5  |
| Fig. S2.....                                                 | 5  |
| Fig. S3.....                                                 | 6  |
| Fig. S4.....                                                 | 6  |
| Fig. S5.....                                                 | 7  |
| Fig. S6.....                                                 | 8  |
| Fig. S7.....                                                 | 8  |
| Fig. S8.....                                                 | 9  |
| Fig. S9.....                                                 | 9  |
| Fig. S10.....                                                | 10 |
| Fig. S11.....                                                | 10 |
| Fig. S12.....                                                | 11 |
| Fig. S13.....                                                | 11 |

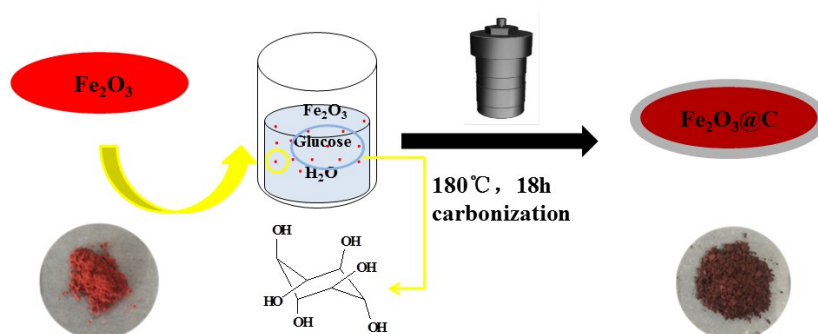
References.....12

## 1. Materials and chemicals

Commercial  $\alpha$ - $\text{Fe}_2\text{O}_3$ , glucose ( $\text{C}_6\text{H}_{12}\text{O}_6$ ), Sodium Acetate (NaAc), Palladium chloride ( $\text{PdCl}_2$ ), Potassium iodide (KI), N, N-dimethylformamide (DMF), Methanol ( $\text{CH}_3\text{OH}$ ) were analytic grade and obtained from Zhongke Kate Industry & Trade Co., Ltd.(Lanzhou, China). All the chemicals were used as received without any further purification. 1 mol/L  $\text{H}_2\text{PdCl}_4$  was synthesized by mixing  $\text{PdCl}_2$  with 36-38% HCl at 70 °C for 1 h. Deionized water (18.25 M $\Omega$ ) was used throughout all the experiment.

## 2. $\alpha$ - $\text{Fe}_2\text{O}_3$ @C preparation

For carbon-coated  $\alpha$ - $\text{Fe}_2\text{O}_3$ , 1.28 g (8mmol)  $\text{Fe}_2\text{O}_3$  and 0.36 g (0.04mmol) glucose were dissolved in 60 ml deionized water, then sonication for 10 min to obtain a highly dispersed mixture. After transferred into a 100 ml Teflon-lined autoclave, the red mixture was heated to 180 °C and held for 48 h. The result red brown materials were collected by centrifugation. After washed with deionized water and absolute ethanol for at least five times, the powder was dried at 80°C for 12h in air. The obtained sample was named  $\text{Fe}_2\text{O}_3$ @C. For comparison, commercial  $\text{Fe}_2\text{O}_3$  support was treated at 180°C for 48h. The schematic of the synthesis process and the morphology of the sample are shown in Scheme S1.



Scheme S1 The schematic of the synthesis process and the morphology of the  $\alpha$ -Fe<sub>2</sub>O<sub>3</sub>@C sample.

### 3. Catalyst characterization

The structures of the crystalline samples were analyzed via X-ray diffraction (XRD) which was collected on an X-ray diffractometer in the  $2\theta$  range from  $10^\circ$  to  $90^\circ$  with steps of  $0.02^\circ$  equipped with Cu K $\alpha$  radiation ( $\lambda = 1.54050 \text{ \AA}$ ). Raman spectra was obtained from a Raman spectrometer Renishaw RM1000 ( $\lambda = 532 \text{ nm}$ ) under ambient conditions. Transmission electron microscope (TEM) micrographs test was collected on a JEM-2010 TEM with an accelerating voltage of 200 KV. The percentage composition of Pd was determined by atomic absorption spectroscopy (AAS) using a ContrAA700 spectrometer. The element composition in the catalysts was collected by X-ray photoelectron spectrometer (XPS) using a ESCALAB 250Xi system with carbonaceous C 1s peak at 284.8 eV as standard. The surface area and pore volume of all the samples were measured using N<sub>2</sub> physisorption at 77 K on a Micromeritics ASAP 2020 instrument and calculated by the Brunauer-Emmett-Teller (BET) method. The samples were degassed at 120 °C for 12 h before measurement. The Fourier transform infrared (FTIR) spectroscopy was obtained using a NEXUS 670 FT-IR spectrometer with KBr pellets prepared by manual grinding. Thermogravimetric (TG) measurement was conducted on a DTG-60H analyzer (Shimadza, Tokyo, Japan) with a heating rate of 10 °C/min. Hydrogen temperature programmed reduction (H<sub>2</sub>-TPR) profiles of the samples were performed on a chemical adsorption instrument TP-5080 with a thermal conductivity detector (TCD). For TPR tests, 60 mg sample was loaded in the quartz tube reactor and pre-treated at 200 °C with an Ar flow (27ml min<sup>-1</sup>) for 1 h and heated up from 30 °C to 900 °C at a heating ramp of 10 °C/min in a 10% H<sub>2</sub>/Ar (1:9) mixture with a flow rate of 30 ml/min. In-situ diffused reflectance infrared Fourier transform spectroscopy (DRIFTS) was recorded by using a VERTEX70 spectrometer equipped with a MCT detector, which was cooled by liquid nitrogen. The catalysts were pretreated under vacuum at

100 °C for 30min, flowing N<sub>2</sub> treated for 30min at room temperature in an in-situ cell reactor. Then the reactant gas (CO or C<sub>2</sub>H<sub>2</sub>) was introduced into the DRIFT cell at 40 °C with a flow rates of 50 mL/min for 15min. The purity of products was confirmed through Gas Chromatography-Mass Spectrometer (GC-MS) on an Agilent 7890A-5975C instrument equipped with a HP-5 MS capillary column (30 m×0.25 mm×0.25 μm). Quantitative analysis was confirmed by GC spectroscopic on a SP-6800A system equipped with a FFAP capillary column (50m×0.32mm×0.50μm). The selectivity of the products is further verified by nuclear magnetic resonance spectroscopy (<sup>1</sup>H NMR), performed on a Bruker 400MHz NMR.

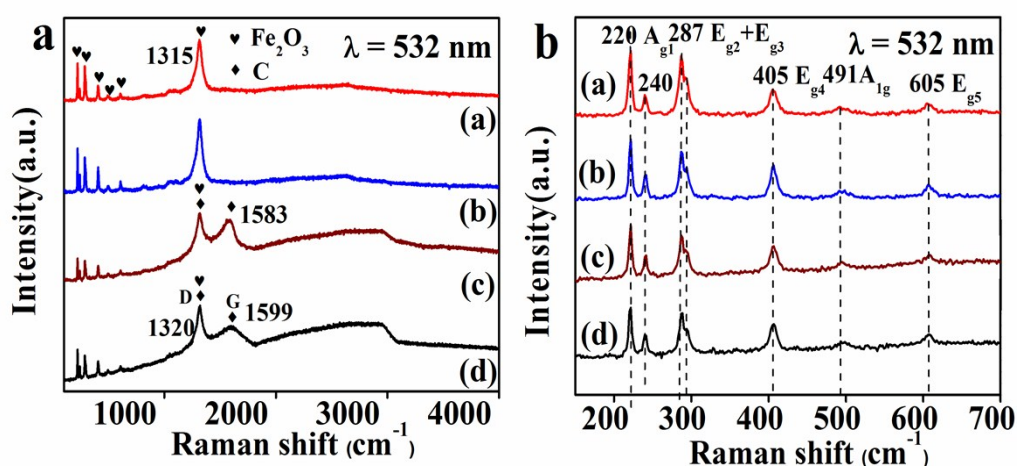


Fig. S1 **a** Raman full spectra and **b** magnified spectra of (a)  $\alpha$ -Fe<sub>2</sub>O<sub>3</sub>, (b) Pd/ $\alpha$ -Fe<sub>2</sub>O<sub>3</sub>, (c)  $\alpha$ -Fe<sub>2</sub>O<sub>3</sub>@C and (d) Pd/ $\alpha$ -Fe<sub>2</sub>O<sub>3</sub>@C.

The peaks in the range of 200–700 cm<sup>-1</sup> could be assigned to the characteristic peaks for  $\alpha$ -Fe<sub>2</sub>O<sub>3</sub>.<sup>1</sup> The bands at 219 and 499 cm<sup>-1</sup> are attributed to the A<sub>1g</sub> mode of  $\alpha$ -Fe<sub>2</sub>O<sub>3</sub> and those observed at 286, 405, and 608 cm<sup>-1</sup> correspond to the E<sub>g</sub> mode of  $\alpha$ -Fe<sub>2</sub>O<sub>3</sub>.<sup>2</sup> The co-presence of  $\alpha$ -Fe<sub>2</sub>O<sub>3</sub> and carbon was further analyzed by Raman spectra. The peaks for  $\alpha$ -Fe<sub>2</sub>O<sub>3</sub>@C (1316 and 1601 cm<sup>-1</sup>) and Pd/ $\alpha$ -Fe<sub>2</sub>O<sub>3</sub>@C (1314 and 1582 cm<sup>-1</sup>) (Fig. S1a) are ascribed to the D (disorder in the carbon structures) and G (graphitic structure) bands of carbon.<sup>3</sup>

The  $I_D/I_G$  ratios increases slightly from 0.74 to 0.80 for  $\alpha\text{-Fe}_2\text{O}_3@\text{C}$  and  $\text{Pd}/\alpha\text{-Fe}_2\text{O}_3@\text{C}$ , suggesting the more defects existence on  $\text{Pd}/\alpha\text{-Fe}_2\text{O}_3@\text{C}$  composite after Pd loading.<sup>4</sup>

Table S1. Physical Properties of  $\alpha\text{-Fe}_2\text{O}_3$ ,  $\alpha\text{-Fe}_2\text{O}_3@\text{C}$ ,  $\text{Pd}/\alpha\text{-Fe}_2\text{O}_3$  and  $\text{Pd}/\alpha\text{-Fe}_2\text{O}_3@\text{C}$

| Sample                                            | Pd loading <sup>a</sup> (wt%) | Carbon content (wt %) <sup>b</sup> | thickness of carbon layers (nm) <sup>c</sup> | $S_{\text{BET}}$ ( $\text{m}^2 \text{g}^{-1}$ ) | $V_{\text{pore}}$ ( $\text{cm}^3 \text{g}^{-1}$ ) |
|---------------------------------------------------|-------------------------------|------------------------------------|----------------------------------------------|-------------------------------------------------|---------------------------------------------------|
| $\alpha\text{-Fe}_2\text{O}_3$                    | --                            | --                                 | --                                           | 4.0237                                          | 0.013381                                          |
| $\alpha\text{-Fe}_2\text{O}_3@\text{C}$           | --                            | 16.10                              | 6                                            | 3.8304                                          | 0.012532                                          |
| $\text{Pd}/\alpha\text{-Fe}_2\text{O}_3$          | 3.45                          | --                                 | --                                           | 1.0153                                          | 0.002306                                          |
| $\text{Pd}/\alpha\text{-Fe}_2\text{O}_3@\text{C}$ | 3.16                          | 15.05                              | 6                                            | 1.102                                           | 0.001102                                          |

<sup>a</sup>Obtained from the AAS result. <sup>b</sup>Obtained from the weight loss of carbon composites based on TG results. <sup>c</sup>Values determined by TEM.

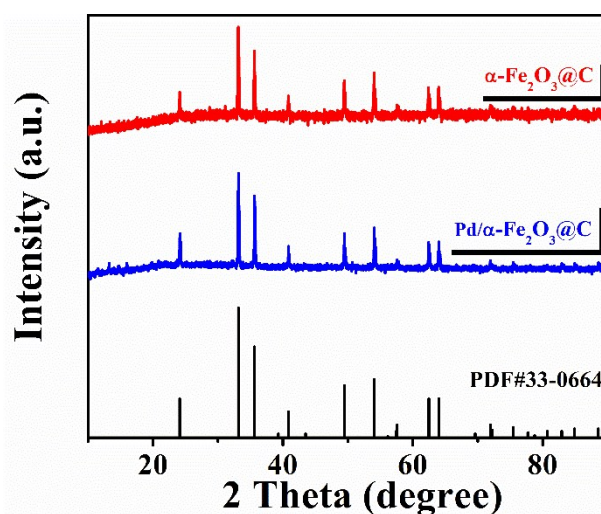


Fig. S2 XRD patterns of  $\alpha\text{-Fe}_2\text{O}_3@\text{C}$  and  $\text{Pd}/\alpha\text{-Fe}_2\text{O}_3@\text{C}$  samples.

The XRD patterns (Fig. S2) of  $\alpha\text{-Fe}_2\text{O}_3@\text{C}$ , there is no peak for carbon could be observed in the spectrum, it might because of its amorphous feature.<sup>5</sup>

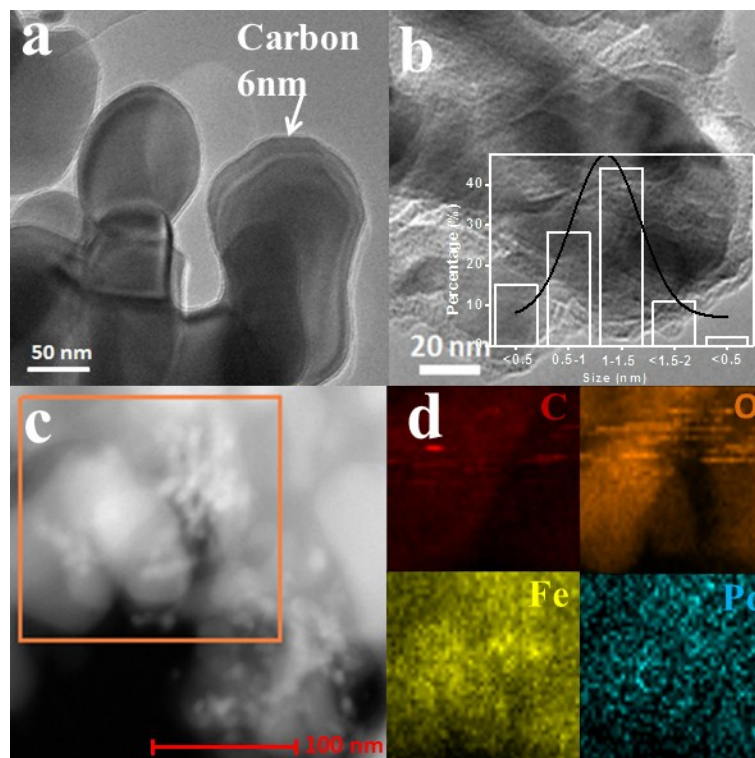


Fig. S3 TEM images **a** of  $\alpha\text{-Fe}_2\text{O}_3@\text{C}$ , **b** and **c** of Pd/ $\alpha\text{-Fe}_2\text{O}_3@\text{C}$ , the particle size distribution of Pd nanoparticles (*inset* in **b**), **d** the elemental mapping of C, O, Fe and Pd in Pd/ $\alpha\text{-Fe}_2\text{O}_3@\text{C}$  catalyst.

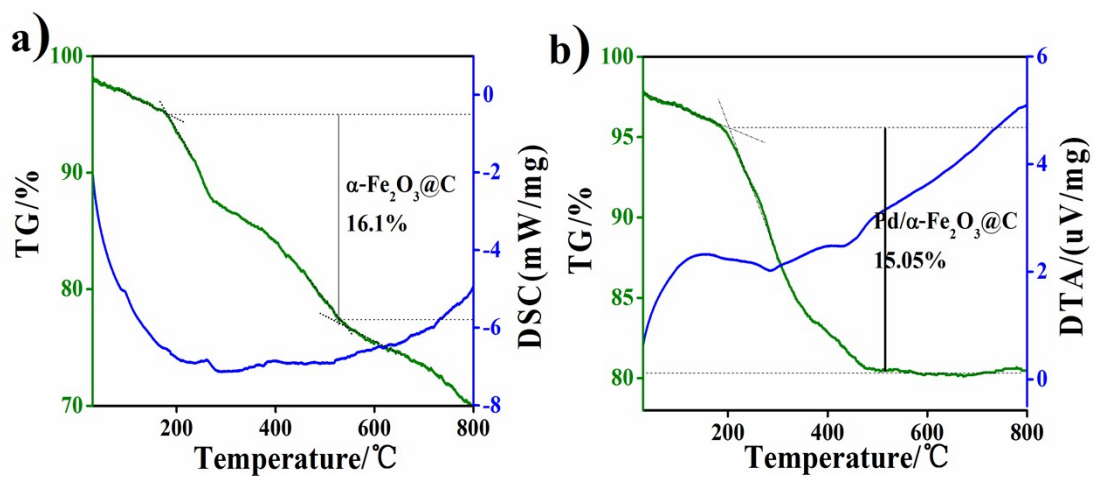


Fig. S4 TGA curves of pure  $\alpha\text{-Fe}_2\text{O}_3@\text{C}$  (a) and Pd/ $\alpha\text{-Fe}_2\text{O}_3@\text{C}$  (b) under air atmosphere with a ramp rate of 5 °C/min.

Thermo gravimetric analysis (TGA) was carried out in air to determine the amount of carbon content. The TGA curve noted that two main weight loss regions co-exist for the sample. The weight loss below 200 °C mainly caused by the loss of adsorbed water, some remaining OH- or carboxyl-groups on the sample, 200 to 400 °C is caused by the consumption of carbon. A gradual weight loss was also observed above 500 °C, which could be ascribed to the thorough decomposition of carbon. The final weight loss percentages were calculated to be 16.1% (Fig. S3a) and 15.05% (Fig. S3b) for  $\alpha$ -Fe<sub>2</sub>O<sub>3</sub>@C and Pd/ $\alpha$ -Fe<sub>2</sub>O<sub>3</sub>@C, respectively.

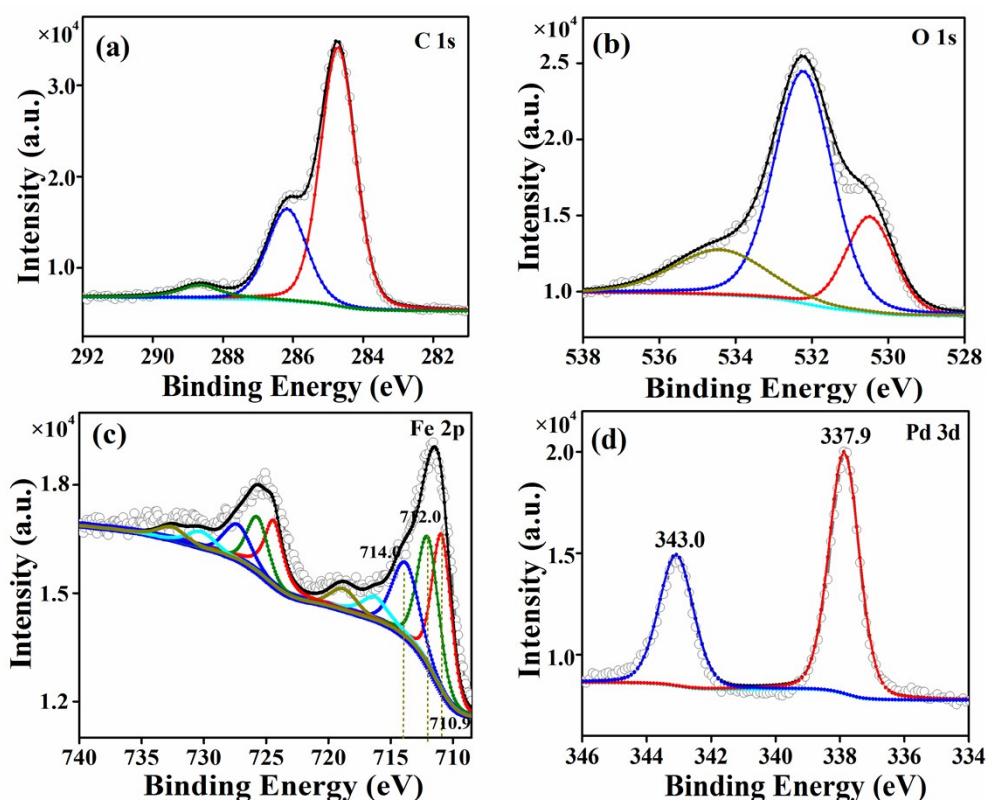


Fig. S5 XPS spectra of Pd/ $\alpha$ -Fe<sub>2</sub>O<sub>3</sub>@C catalyst: (a) C 1s, (b) O 1s, (c) Fe 2p and (d) Pd 3d.



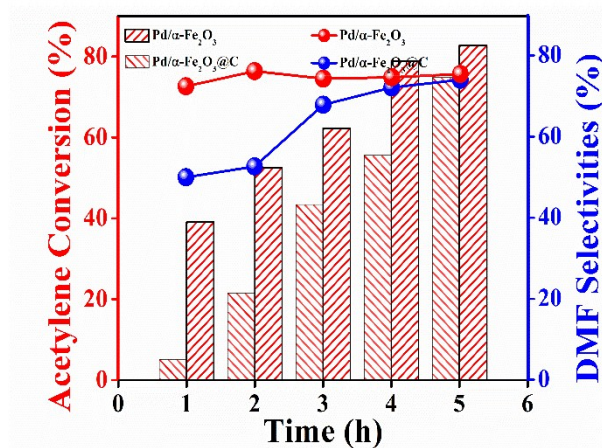


Fig. S6 The reaction rate over Pd/α-Fe<sub>2</sub>O<sub>3</sub> and Pd/α-Fe<sub>2</sub>O<sub>3</sub>@C catalysts for acetylene dicarbonylation. Reaction conditions: 50 mg catalyst, 10 mmol CH≡CH, O<sub>2</sub>+CO (1:10, 5MPa), KI as promoter, 80°C.

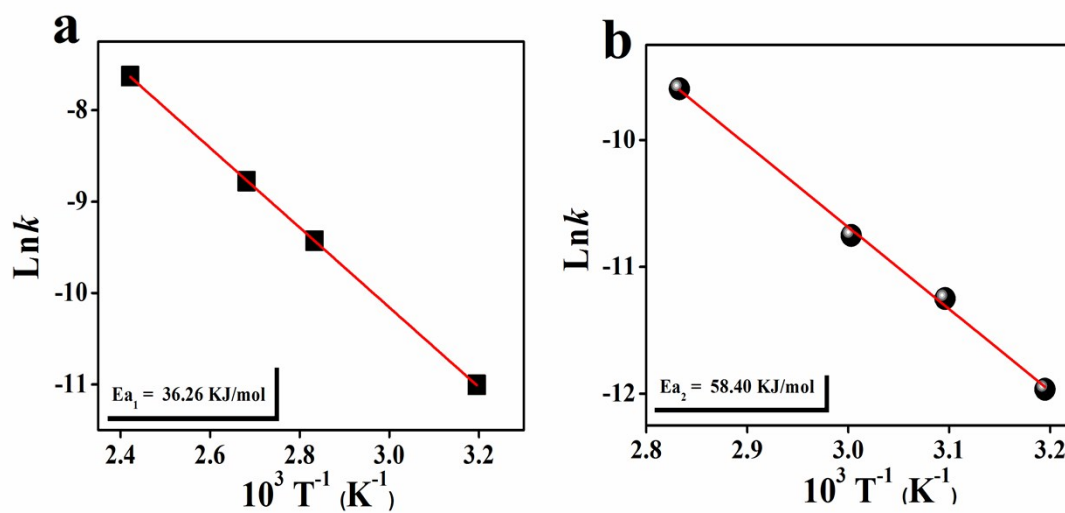


Fig. S7 Arrhenius plots for acetylene dicarbonylation over (a) Pd/α-Fe<sub>2</sub>O<sub>3</sub> and (b) Pd/α-Fe<sub>2</sub>O<sub>3</sub>@C in the temperature range of 40–140°C.

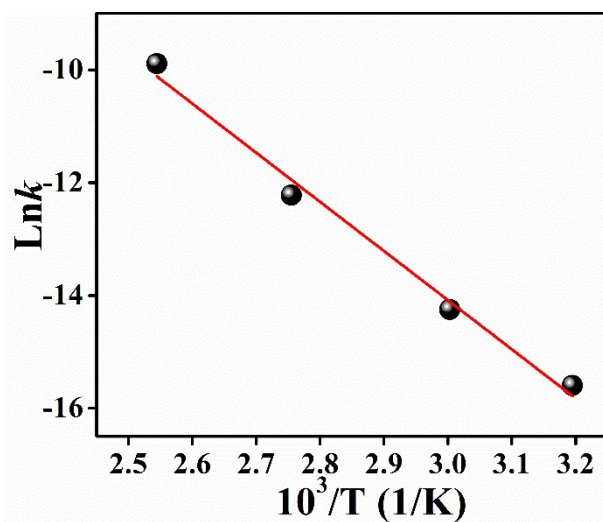


Fig. S8 Arrhenis plots for acetylene dicarbonylation over Pd/C in the temperature range of 40–120 °C.

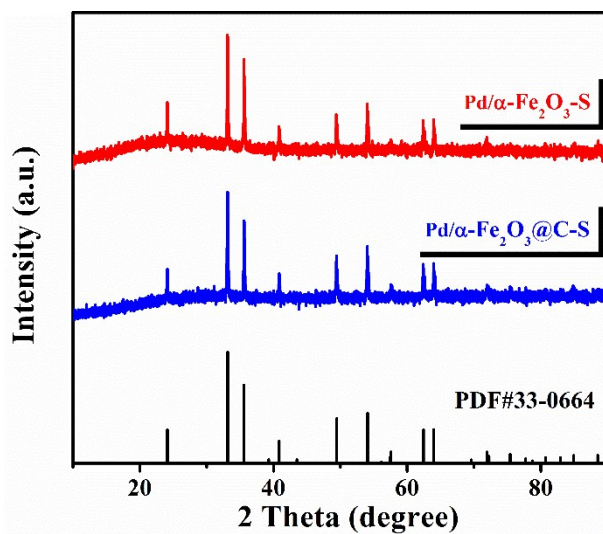


Fig. S9 XRD patterns of Pd/ $\alpha$ -Fe<sub>2</sub>O<sub>3</sub>-S and Pd/ $\alpha$ -Fe<sub>2</sub>O<sub>3</sub>@C-S samples.

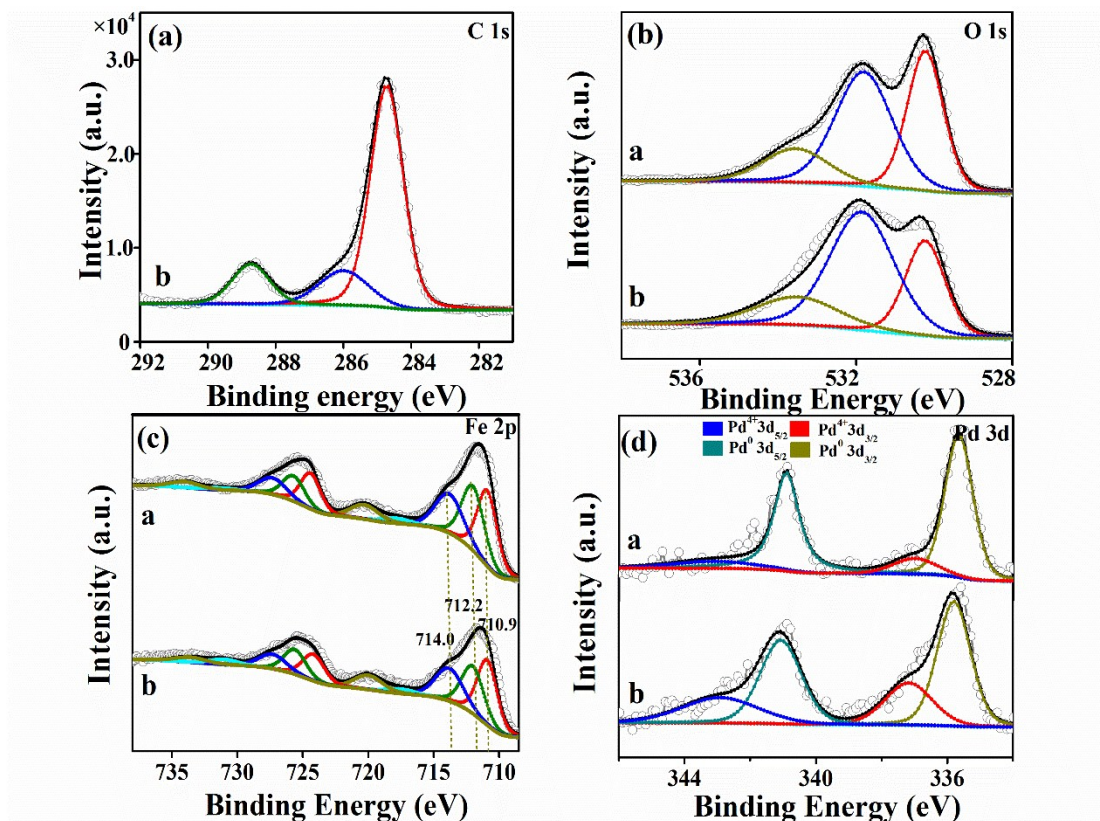


Fig. S10 XPS spectra of spend **a** Pd/ $\alpha$ -Fe<sub>2</sub>O<sub>3</sub> and **b** Pd/ $\alpha$ -Fe<sub>2</sub>O<sub>3</sub>@C catalyst: (a) C 1s, (b) O 1s, (c) Fe 2p and (d) Pd 3d.

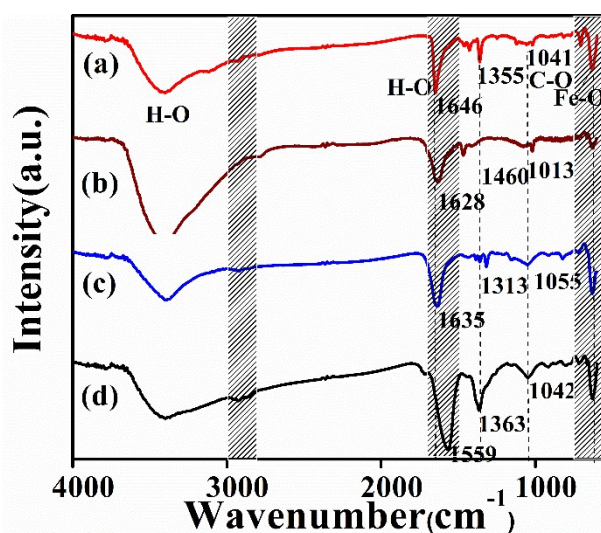


Fig. S11 FT-IR spectra of Pd/ $\alpha$ -Fe<sub>2</sub>O<sub>3</sub> (a), Pd/ $\alpha$ -Fe<sub>2</sub>O<sub>3</sub>@C (b), Pd/ $\alpha$ -Fe<sub>2</sub>O<sub>3</sub>-S (c) and Pd/ $\alpha$ -Fe<sub>2</sub>O<sub>3</sub>@C-S (d).

In the FT-IR spectra, all samples show a broad band at 500-650  $\text{cm}^{-1}$ , which could be attributed to the vibration of Fe-O bond. As for all samples, the characteristic signal of Pd-O bond stretch at 1415  $\text{cm}^{-1}$  is observed,<sup>6</sup> with the strength decrease after used, indicating the decomposition of PdO during the process, which is in well agreement with the XPS results.

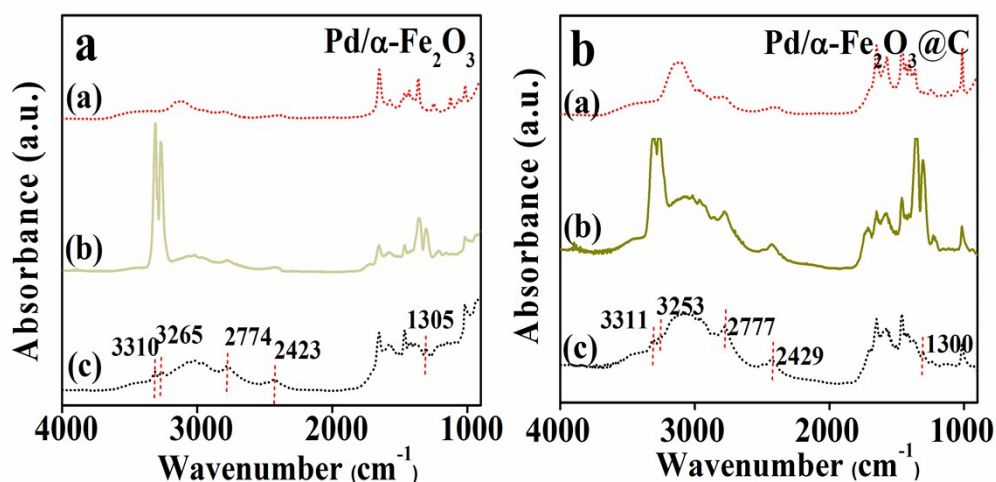


Fig. S12 In situ DRIFTS spectra for  $\text{C}_2\text{H}_2$  adsorption over **a**  $\text{Pd}/\alpha\text{-Fe}_2\text{O}_3$  and **b**  $\text{Pd}/\alpha\text{-Fe}_2\text{O}_3@\text{C}$  catalysts.

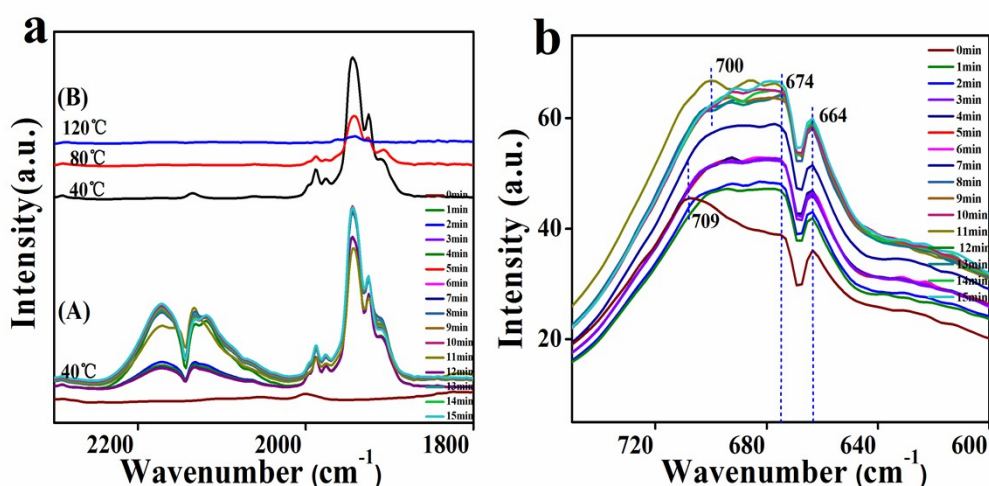


Fig. S13 In situ DRIFTS spectra for CO adsorption over  $\text{Pd}/\alpha\text{-Fe}_2\text{O}_3$ . (a) 40  $^\circ\text{C}$  adsorption curve (A) and 40, 80, 120  $^\circ\text{C}$  desorption curve for 1 min (B); (b) Magnification curve of adsorption curve within 15 minutes.

## References

1. K. F. Zhao, H. L. Tang, B. T. Qiao, L. Li, J. H. Wang, *ACS Catal.*, 2015, **5**, 3528-3539.
2. Y. F. Jian, T. T. Yu, Z. Y. Jiang, Y. K. Yu, M. Douthwaite, J. Y. Liu, R. Albilali, C. He, *ACS Appl Mater Interfaces*, 2019, **11**, 11369-11383.
3. Y. Wang, X. M. Guo, Z. K. Wang, M. F. Lü, B. Wu, Y. Wang, C. Yan, A. H. Yuan, H. X. Yang, *J. Mater. Chem. A*, 2017, **5**, 25562-25573.
4. T. Han, Y. Wei, X. Z. Jin, H. F. Jiu, L. X. Zhang, Y. Sun, J. Tian, R. R. Shang, D. L. Hang, R. Zhao, *J. Mater. Sci.*, 2019, **54**, 7119-7130.
5. M. Y. Zhu, J. R. Kan, J. M. Pan, W. Z. Tong, Q. Chen, J. C. Wang, S. J. Li, *J. Ener. Chem.*, 2019, **28**, 1-8.
6. H. Z. Tan, Z.-N. Chen, Z. N. Xu, J. Sun.; Z. Q. Wang, R. Si, W. Zhuang, G. C. Guo, *ACS Catalysis*, 2019, **9**, 3595-3603.